Heliyon 6 (2020) e03713

Contents lists available at ScienceDirect

Heliyon

journal homepage: www.cell.com/heliyon

Research article

Strain effects on the electronic, optical and electrical properties of Cu_2ZnSnS_4: DFT study

S. Kahlaoui [a,b,*], B. Belhorma [b], H. Labrim [b], M. Boujnah [c], M. Regragui [a]

[a] MANAPSE, Faculty of Sciences, Mohammed V University, B. P. 1014, Rabat, Morocco
[b] Materials Science Unit/DERS/National Centre for Energy, Sciences and Nuclear Techniques (CNESTEN), Rabat, Morocco
[c] LAMCSCI, Faculty of Sciences, Mohammed V University, B. P. 1014, Rabat, Morocco

ARTICLE INFO

Keywords:
Condensed matter physics
Materials science
Physical chemistry
Thermodynamics
CZTS
Photovoltaic conversion
Compression
Dilatation
Electrical conductivity
Density of states

ABSTRACT

Based on the density functional theory and Boltzmann transport theory, we investigated electronic, electrical and optical properties of Kesterite CZTS under different strain conditions. Our results indicate that both biaxial compressive and tensile strain effects lead to change in the band gap of this structure with different strain values. Furthermore, the edge of absorption, under the influence of an increasing compression, moves towards the short wavelengths. Electrical conductivity for pure CZTS and under dilatation and compression shows that with the increase of dilatation the conductivity of the material also increases, this physical property could be exploited to improve the performance of CZTS a suitable absorbent material in solar cells.

1. Introduction

During the last decade many research and development studies have focused on renewable energy, in particular solar energy conversion through photovoltaic cells. Photovoltaic conversion of solar energy occurs in semiconducting materials which have the property of releasing their charge carriers (electrons and holes) after absorption of photons and heat from sunlight. Such conversion is based on photovoltaic effect [1]. These technologies have reached an industrial stage using cells based on crystalline silicon. However, a large number of scientists are working on other materials such as Cu (In, Ga) Se_2 and CdTe [2, 3] thin film solar cells to save the active materials and the energy used in their manufacturing. The efficiency for these technologies is over 20% [4]. Unfortunately, these materials are based on elements that are rare, expensive or toxic which could compromise their development. To alleviate this drawback many research efforts have been done on the development of thin film solar cells composed of abundant and non-toxic elements such as Cu_2ZnSnS_4 (noted CZTS) [5, 6]. It has interesting optical and electrical properties such as a band gap of 1.5 eV and a high absorption coefficient (10^4 cm^{-1}) [7,8]. The latest efficiency records with CZTS (Se) absorbers reach 12.6% [9]. In experimental studies, various procedures have been applied for CZTS thin film fabrication using different methods of deposition techniques such as: sol-gel [10, 11], electroplating [12, 13], spray pyrolysis [14], pulsed laser deposition [15, 16], co-evaporation [17] etc. In addition, there are also some reports on theoretical studies of CZTS which have presented a reasonable understanding of the stable Kesterite crystalline and electronic structures of CZTS [18, 19]. Chun-Ran Li reported the first principle calculations of Cu_2ZnSnS_4 (CZTS) under biaxial strain, where electrical properties were systematically investigated using CASTEP code based on generalized gradient approximation and hybrid functional method; he found that the change trend of optical band gap is consistent with fundamental band gap under biaxial strain [20].

However, strain effect is a potential tool for altering the atomic positions and defect formations. It can adjust the electronic structures and lattice vibrations. It can also affect the phase transition of the structure, and phase transformation inevitably as well as in the physical and chemical properties. Consequently, the use of the strain plays an important role in the material properties. To the best of our knowledge, research on electronic, optical and electrical properties of CZTS under compression and dilatation has not been previously reported. These strains have an important effect on this material, so exploring the electronic, optical and electrical properties of CZTS is of great importance to illuminate the properties of CZTS.

* Corresponding author.
E-mail address: sa.kahlaoui@gmail.com (S. Kahlaoui).

https://doi.org/10.1016/j.heliyon.2020.e03713
Received 12 March 2019; Received in revised form 7 September 2019; Accepted 27 March 2020

Table 1. Wyckoff positions of compound Cu_2ZnSnS_4.

Cu à 2a	**0**	**0**	**0**
Cu à 2c	0	0.5	0.25
Zn à 2d	0	0.5	0.75
Sn à 2b	0	0	0.5
S à 8g	0.7562	0.2434	0.12821

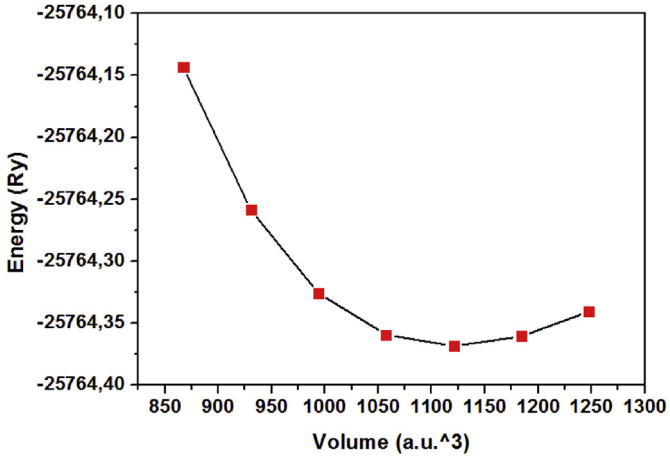

Figure 1. The variation of total energy as a function of volume.

This paper reports the first-principle calculations results of the effects of biaxial strain on the electronic, optical, structural and electrical properties of CZTS using Tran Blaha-Johnson (mBJ) method [21].

This paper is organized as follows: in Section 2 we give the computational details and brief description of calculation method. The theoretical results description and discussion are presented in Section 3. Finally conclusions are mentioned in Section 4.

Table 2. Equilibrium lattice parameters of CZTS corresponding to the minimal total energy (under biaxial strain).

		$a = b$ (Å)	E_t (Ry)	$c = c_0$ (Å)
Pure	0%	5.49	-25764.36	10.98
Dilatation	2%	5.60	-25764.33	10.98
	4%	5.70	-25764.30	10.98
	6%	5.81	-25764.28	10.98
Compression	-2%	5.38	-25764.33	10.98
	-4%	5.27	-25764.30	10.98
	-6%	5.16	-25764.28	10.98

Table 3. Equilibrium lattice parameters of CZTS corresponding to the minimal total energy (under uniaxial strain).

		$a = a_0 = b_0$ (Å)	E_t (Ry)	c (Å)
Pure	0%	5.49	-25764.36	10.98
Dilatation	2%	5.49	-25764.35	11.19
	4%	5.49	-25764.34	11.41
	6%	5.49	-25764.33	11.63
Compression	-2%	5.49	-25764.35	10.76
	-4%	5.49	-25764.34	10.54
	-6%	5.49	-25764.33	10.32

2. Computational methods

The First-principles calculations are performed with full potential linearized augmented plane (FP-LAPW) method, as implemented in WIEN2K code [22], using the Tran-Blaha modified Becke-Johnson (TB-mBJ) potential [23] to describe the effect of the exchange and correlation function [24]. The advantage of this method is to improve band gaps obtained by the conventional density functional theory (DFT)-based methods, which provide the results for wide band gap insulators, sp semiconductors, 3d transition-metal oxides [25, 26] half-metallicity [27, 28] and doped semiconductor systems [29, 30]. Tran and Blaha tested the exchange potential proposed by Becke and Johnson (BJ) [23] which was designed to reproduce the exact exchange potential form "the Optimized effective potential" (OEP). They found that the use of the BJ potential combined with the correlation potential of the LDA always results in underestimated gap energies. In order to improve these results, Tran and Plaha introduced a simple modification of the original BJ potential and achieved good agreement with other more expensive approaches (due to their high self-alignance) such as hybrid functions and the GW method. The modified BJ potential (Mbj) proposed by Tran and Blaha has the following form:

$$\upsilon_{\times\sigma}^{MBJ}(r) = c\upsilon_{\times,\sigma}^{BR}(r) + (3c-2)\frac{1}{\pi}\sqrt{\frac{5}{12}}\sqrt{\frac{2t_\sigma(r)}{\rho_\sigma(r)}} \quad (1)$$

where $\rho(r)$ is the density of electrons, $t_{(r)}$ is the density of kinetic energy and $\upsilon_{\times\sigma}^{MBJ}$ is the potential of Becke-Roussel (BR) [Becke (1989)] which was proposed to model the coulombian potential created by the exchange hole. The index σ is the spin rating.

In Eq. (1) c was chosen to depend linearly on the square root of the average of $\frac{|\nabla\rho(r')|}{\rho(r')}$ and

$$c = \alpha + \beta\left(\frac{1}{Vc_{ell}}\int_{c_{ell}}\frac{|\nabla\rho(r')|}{\rho(r')}\,d^3\,r'\right)^{1/2} \quad (2)$$

where Vc_{ell} is the unit cell of volume, in Eq. (2) α and β are two free parameters whose values are: $\alpha = -0.012$ and $\beta = 1.023$ $\text{bohr}^{1/2}$ according to a fit to the experimental band gaps.

For $c = 1$, the original BJ potential is reproduced. By varying c for a given material, it was found that for several solids, the gap energy increases in a monotonous way compared to c. Specifically, for solids with small gaps, C_{opt} extends from (1.1–1.3) whereas for solids of a larger gap, C_{opt} is larger (its value varies from 1.4 to 1.7) [23].

In the (FP-LAPW) method, the unit cell is specified in two regions: Rmt radius spheres (muffin-tin-like spheres) (spheres that do not overlap and are centered on each Rmt radius atom).the interstitial region (the remaining region). Wave functions, electronic densities and potential are developed in combination of spherical harmonics multiplied by the radial functions around atomic sites, that is, in the spheres muffin-tin with cut-off radius (cut-off) of Lmax = 10, Also we use the value 7 of (Rmt × Kmax); Rmt is the smallest muffin-tin radius and Kmax is the cutoff for the plane wave). The first step is to specify the values of the important parameters that affect the time and accuracy of the calculation: Rmt values [muffin-tin sphere radius, unit data atomic (u.a)] that we have used represent a good choice for the calculation. This choice is based on two criteria:

1 Ensure the integration of the majority of the electrons of the heart into the sphere (Muffin-tin).
2 Avoid overlapping spheres (Muffin-tin).

The cut-off parameter (Rmt × Kmax), used for the development in plane waves of own functions. Gmax = 12 is the standard of the largest wave vector used for the development of load density in plane waves. The 2 × 2 × 2 division for k-point sampling was used and the tetrahedral

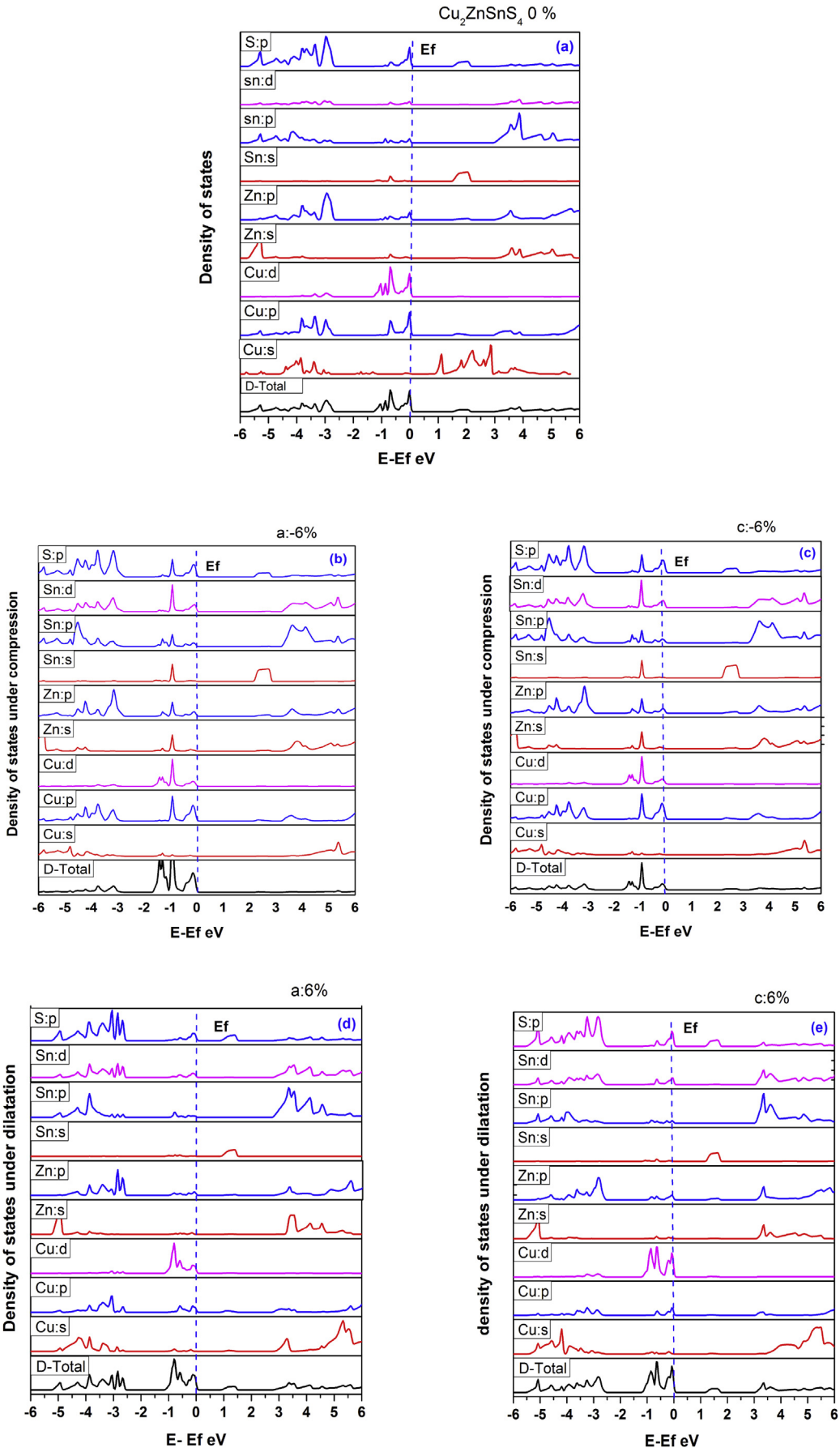

Figure 2. Total and partial density of state for Cu_2ZnSnS_4 pure (a), and under (c–e) uniaxial and (b–d) biaxial strains.

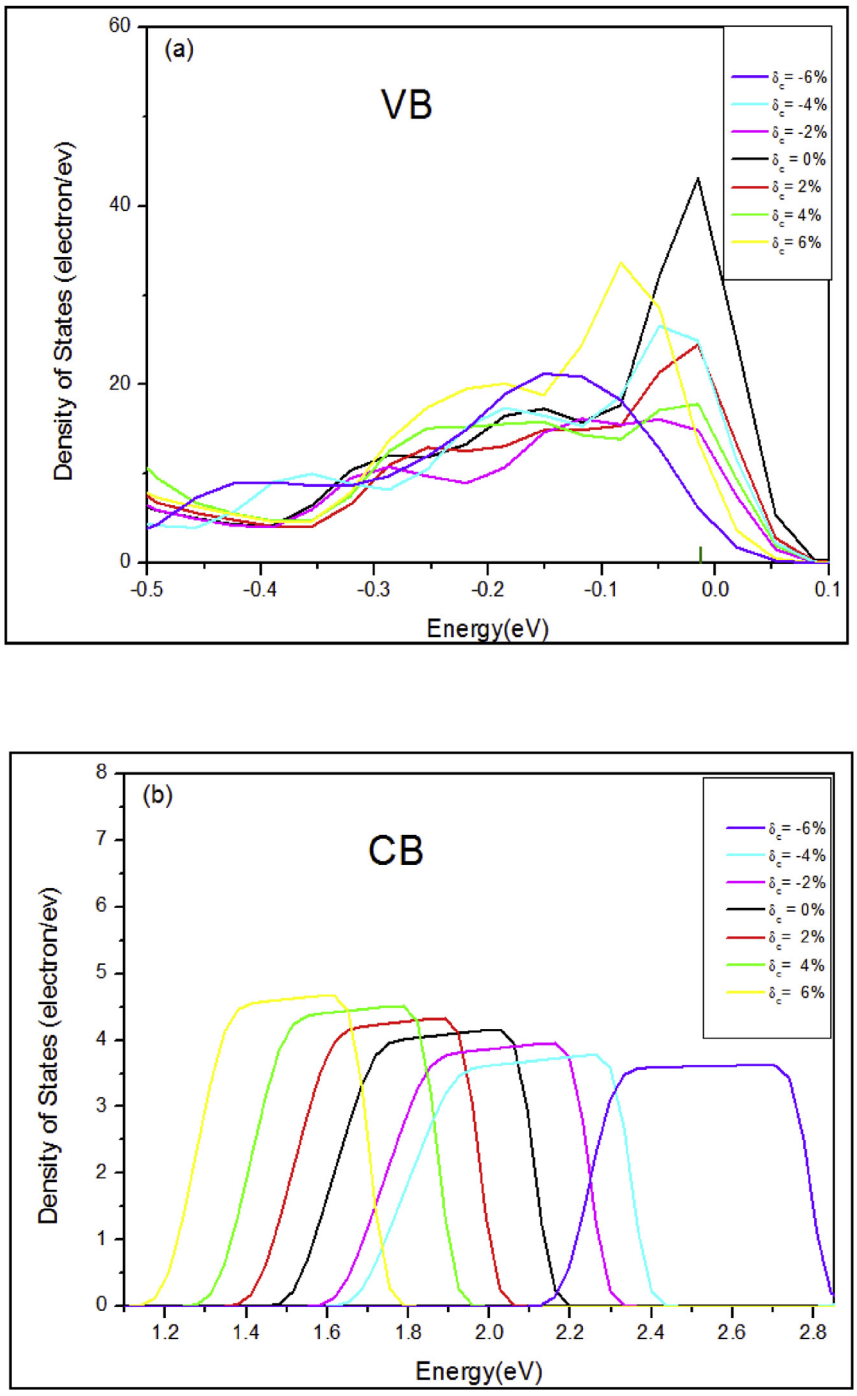

Figure 3. The density of states under uniaxial strains for the (a) VB and (b) CB. The Fermi energy level is shifted to 0 eV.

method [31] was employed for the Brillouin zone integrations. A number of iterations (40) are dedicated to accomplishing self-consistency. The muffin tin radii for Zn, Cu, Sn and S are chosen to be 2.19, 2.20, 2.26 and 1.79 a.u respectively. Structural optimization involves determining the fundamental condition. The iteration process is repeated until total energy is stable at 10^{-5}Ry.The energy that separates the states of valence and those of the core was taken equal to -6 Ry. Electronic configurations used in our calculations as values for the atoms are: Zn ($3d^{10}$ $4s^{2}$), Cu ($3p^{6}$ $4s^{2}$ $3d^{9}$), Sn ($4d^{10}$ $5s^{2}$ $5p^{2}$) and S ($3s^{2}$ $3p^{4}$).

The definition of these strains parallel to a, and c-axis can be found in Ref. [32]. The biaxial and uniaxial in-plane strain is defined by (Eqs. (3) and (4)):

$$\delta_a = \delta_b = \frac{a - a_0}{a_0} \times 100\% \ \ biaxial\ strain \tag{3}$$

$$\delta_c = \frac{c - c_0}{c_0} \times 100\% \ \ uniaxial\ strain \tag{4}$$

where $a_0 = b_0$ and c_0 is the optimized lattice constants of the unstrained bulk Cu_2ZnSnS_4, and $a = b$, c is the in-plane lattices constants of bulk Cu_2ZnSnS_4 under strain. The electrical coefficients are derived using the semi-classical Boltzmann theory as implemented in the Boltzmann (BoltzTraP) program [33].

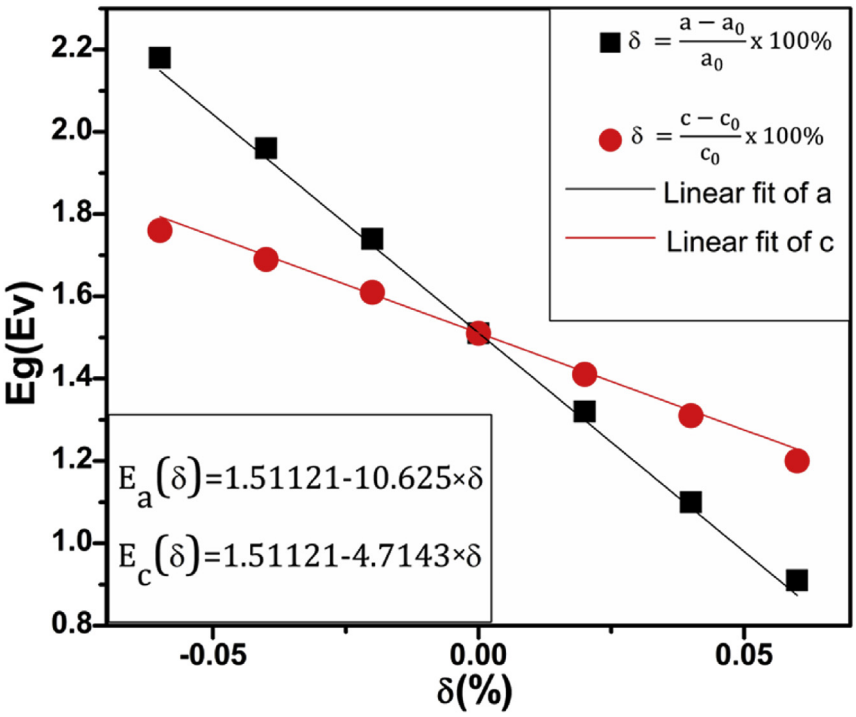

Figure 4. Optical band gap as a function of in-plane biaxial strains following a and b axis and uniaxial strain following c axis.

3. Results and discussions

3.1. Geometry optimization

Before presenting our results for strained CZTS, we first discuss, the unstrained CZTS of kesterite structure (I-4; No.82) [34,35] by comparing our results with experimental works [36, 37]. This structure is characterized by the cations in a and b sites and anion in d, the positions 2a, 2b, 2c and 2d are in both cases occupied respectively by Cu, Sn, Cu and Zn. Thus the cations form planes normal to the lattice constant c, on which Cu/Zn occupy the plane 2c/2d and the plane 2a/2b is occupied by Cu/Sn. These cation planes are related chalcogen planes on the 8g position. (see Table 1).

Total energy as a function of volume for kesterite CZTS is presented in Figure 1 where the total energy is fitted by the Murnaghan's Eq. (5) [38].

$$E(V) = E_0 + \frac{B_0 \times V}{B'_0}\left[\frac{(V_0/V)^{B'_0}}{B'_0 - 1} + 1\right] - \frac{B_0 \times V}{B'_0 - 1} \quad (5)$$

where V_0 is the equilibrium volume, E_0 is the equilibrium energy, B_0 the bulk modulus, and is B'_0 the first derivative of E_0 with respect to pressure.

From this equation we determine the lattice parameters ($a_0 = b_0$ and c_0) corresponding to the minimal energy. The obtained values of these parameters are $a_0 = 5.49$ Å and $\frac{c_0}{a_0} = 2$; this result is in accordance with reported experimental values of $a_0 = 5.42$ Å and $\frac{c_0}{a_0} = 2$ respectively [39, 40, 41]. This accordance confirms that the used calculation method is correct; then, the same method is followed for the rest of the work presented in this article

In this part, using mBJ method [21], the effect of strain ranging from $\delta = -6\%$ to $\delta = +6\%$ on physical properties, where negative and positive values represent compression and dilatation respectively were analyzed. The equilibrium lattice parameters corresponding to the minimal total energy are shown in Tables 2 and 3 for pure compound without strain as well as effects of, dilatation and compression. A biaxial strain is applied at a first time simultaneously on a and b axis while the structure is maintained unconstrained on c direction; and at a second time, the strain is applied on c axis while the structure is maintained unconstrained on a and b directions.

The results show that the t\otal energy of system increases with both increasing the compressive strain (from 0% to −6%) and tensile strain (from 0% to 6%). As we can see, the minimum strain energy is located at $\delta = 0\%$.

3.2. Electronic properties

3.2.1. Density of states

The electronic properties of CZTS with and without strain are performed for a series of uniaxial and biaxial strains values from -6% to +6%. The obtained results show similar behavior for the total and partial density of states (DOS) with a shift on pic positions illustrated in Figure 2 For clarity, the DOS for $\delta = -6\%, 0\%$ and $+6\%$ were represented.

In this part the effect of a compression or tensile strains, which causes a variation of the parameters a = b and c which increase under biaxial and uniaxial compression and shrink under tensile were studied as shown in Tables 2 and 3.

The VB (Valence Band) was divided into two regions. The first region of the lower energy [-5.71eV, -2.66eV] contains contribution of Cu-d, Cu-p, Zn-p and S-p states, the second region [-1.32eV; 0eV] is dominated by Cu-d, Cu-p, Sn-p, Sn-d, Zn-p and S-p states. The CB (Conduction Band) minima contains only contributions of Cu-s states. See (Figure 2a).

From the DOS of Figure 2(b, c, d and e), the imposed compression and dilatation affected the band gap of Cu_2ZnSnS_4. Just below the Fermi level, the valence bands are dominated by the S-p, Cu-d and Cu-p states. However, the Cu-p state contribution becomes less visible under dilatation, whereas Cu-s has shifted away from the CB minima towards higher energy.

To illustrate the effect of strain on the gap energy, we inspect the total DOS of the valence band VB maxima and the conduction CB band minima (see Figure 3). It is clear to see that the VB minima is almost not effected by the applied uniaxial (Figure 3a), or biaxial strain, which is supported by DOS of these systems under biaxial and uniaxial strains. Whereas the energy gap variations are mainly induced by the changes of the CB

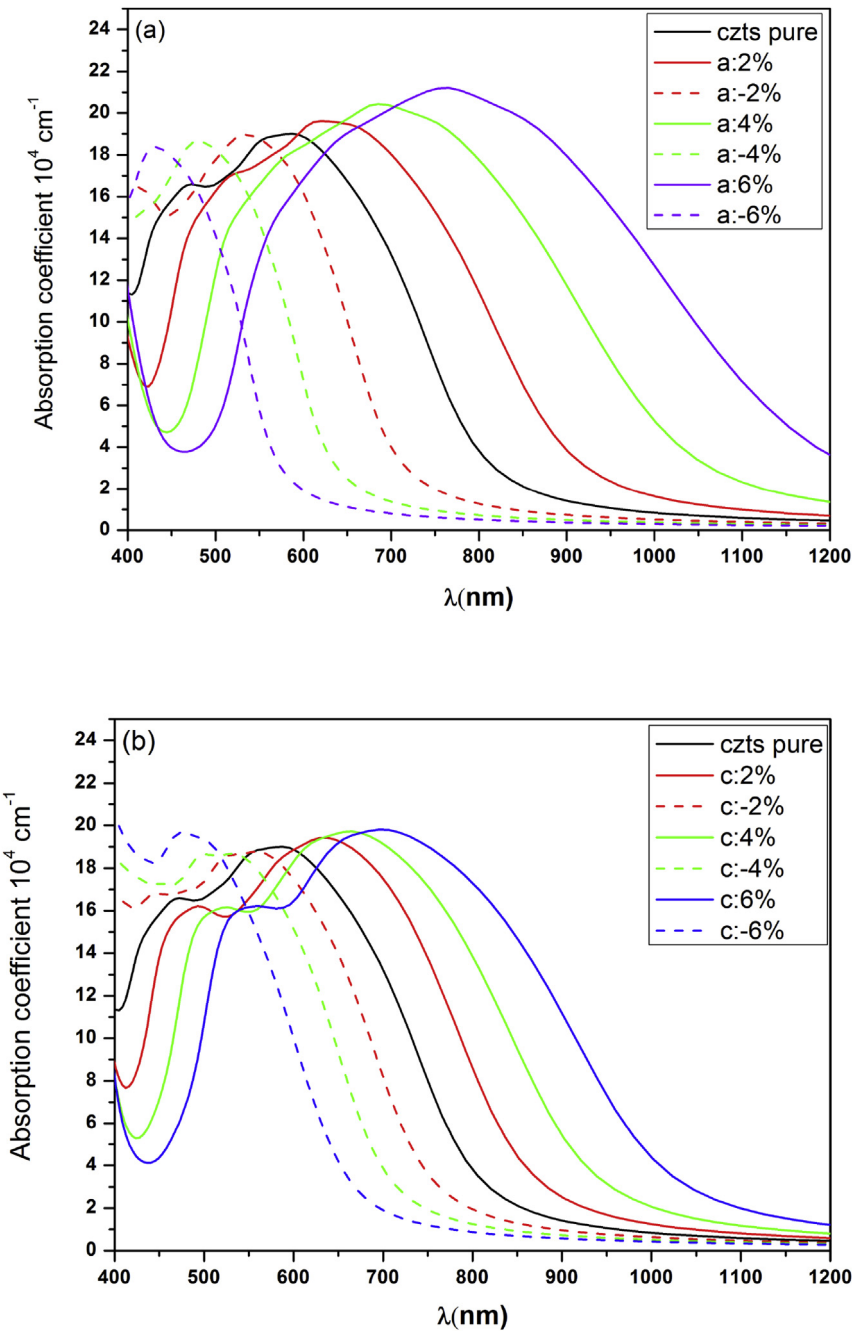

Figure 5. Relation between the absorption and wavelengths for the (a) under different biaxial strains following a and b axis and for the (b) under different uniaxial strains following c axis.

minima that decrease linearly with the applied uniaxial (Figure 3b) strain from $\delta = -6\%$ to $\delta = +6\%$.

3.3. Optical properties

To confirm what is shown in the density of states in the electronic properties Section, the variation of band gap as a function of in-plane biaxial strains and uniaxial strain were plotted as shown in Figure 4. The unstrained band gap of CZTS calculated by mBJ method is 1.51 eV, which is consistent with reported experimental results [42, 43].

It can be found that the band gap of CZTS decreases linearly while the uniaxial or biaxial tensile strain increase. Under the applied uniaxial tensile strain $\delta_c = +6\%$, the band gap of CZTS decreases to a minimum value of 1.2 eV. But for the uniaxial compressive strain, the energy gap of CZTS reach 1.76 eV under $\delta_c = -6\%$. Similar phenomenon also occurs in the situation of biaxial strain, the band gap of the considered system decreases linearly to 0.91 eV while increasing the biaxial tensile strain to $\delta a = \delta b = +6\%$. For the biaxial compressive strain, the energy gap of CZTS increases to 2.18 eV unde $\delta_a = \delta_b = -6\%$.

The variation of Eg vs δ is linear and can be fitted by a linear function (Eqs. (6), (7), and (8)).

$$E(\delta) = A + B \times \delta \tag{6}$$

$$Eg(\delta) = 1.511 - 10.625 \times \delta a \text{ for a and b axis strain} \tag{7}$$

and

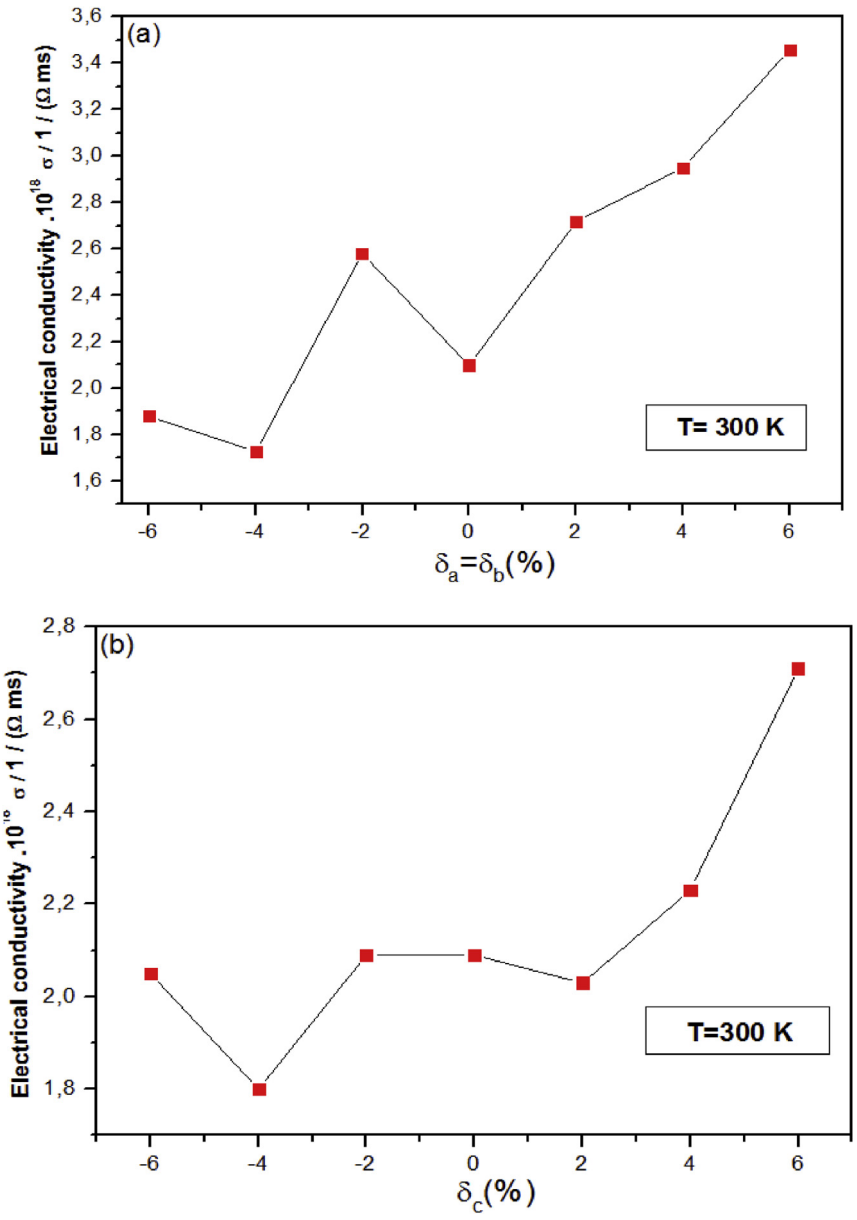

Figure 6. Electrical conductivity for the (a) as a function of in-plane biaxial strains following a and b axis and for the (b) uniaxial strain following c axis.

$Eg(\delta) = 1.511 - 4.714 \times \delta c$ for c axis strain (8)

Absorption spectra of semiconductors show that the optical absorption falls rapidly towards the infrared. The photon energy, at the absorption threshold (maximum energy of absorption edge) corresponds to the bands gap Eg found by other methods [44, 45]. If we submit the crystal to a variable (strain-stress) then we find that the absorption curve moves towards the big or the short wavelengths.

The displacement of the value extrapolated for absorption edge gives a direct measure of the change of Eg with compression or tension. For the CZTS, the edge of absorption, under the influence of an increasing compression, moves towards the short wavelengths; and furthermore the curves move to high wavelengths under dilatation (Figure 5).

The value of absorption increases corresponding to increasing the strain from −6% to +6% **(see (**Figure 5a **and** Figure 5b**).** The phenomena could be attributed to the decrease of the electronic transition energy with the strain, which results in more photons being absorbed.

The calculated electrical conductivities for both cases are shown in (Figure 6a and Figure 6b) it is calculated by using BoltzTrap code [33] implemented in the WIEN2k package. The theoretical Boltzmann method is described in this study [46].

The results show that with an increase in dilatation the conductivity of the material also increases and reaches its maximum.

The dilation of the material corresponds to increase of the interatomic distance, which leads to a fragility of bonds, which consequently facilitates their breaking and thereafter generates an increase of free charges and an increase in electrical conductivity.

4. Conclusion

In this paper the main structural parameters that influence the electrical and optical properties of CZTS as a material for photovoltaic application were studied. The effect of a compression or tensile strains were followed by variation of the lattice parameters a and c which increase under biaxial compression and shrink under tensile. The unstrained band gap calculated by mBJ method of CZTS is 1.51eV, which is consistent with the reported experimental results. The band gaps increased with increasing compression as well as decreased by increasing

dilation following both a and c axes. Absorption spectra of semiconductors show that the optical absorption under strain falls rapidly towards the infrared. The calculated electrical conductivity indicates that when increasing dilatation the conductivity of the material also increases.

Declarations

Author contribution statement

S. Kahlaoui: Conceived and designed the experiments; Performed the experiments; Analyzed and interpreted the data; Contributed reagents, materials, analysis tools or data; Wrote the paper.

B Belhorma: Analyzed and interpreted the data.

H. Labrim: Conceived and designed the experiments.

M. Boujnah: Contributed reagents, materials, analysis tools or data.

M. Regragui: Analyzed and interpreted the data.

Funding statement

This research did not receive any specific grant from funding agencies in the public, commercial, or not-for-profit sectors.

Competing interest statement

The authors declare no conflict of interest.

Additional information

No additional information is available for this paper.

References

[1] X. Mathew, V.P. Singh, Photovoltaics, solar energy materials and thin films - IMRC 2008, Cancun, Mexico, Thin Solid Films 518 (7) (Jan. 2010) 1763.

[2] A. Romeo, et al., Development of thin-film Cu (In,Ga)Se_2 and CdTe solar cells, Prog. Photovoltaics Res. Appl. 12 (23) (2004) 93–111.

[3] J.H. Shi, Z.Q. Li, D.W. Zhang, Q.Q. Liu, Z.Z. Sun, S.M. Huang, Fabrication of Cu(In, Ga)Se_2 thin films by sputtering from a single quaternary chalcogenide target, Prog. Photovoltaics Res. Appl. 19 (2) (2011) 160–164.

[4] L. Yalçin, R. Öztürk, Performance comparison of c-Si, mc-Si and a-Si thin film PV by PVsyst simulation, J. Optoelectron. Adv. Mater. 15 (3–4) (2013) 326–334.

[5] W. Ki, H.W. Hillhouse, Earth-abundant element photovoltaics directly from soluble precursors with high yield using a non-toxic solvent, Adv. Energy Mater. 1 (5) (2011) 732–735.

[6] K. Woo, Y. Kim, J. Moon, A non-toxic, solution-processed, earth abundant absorbing layer for thin-film solar cells, Energy Environ. Sci. 5 (1) (2012) 5340–5345.

[7] S. Macavei, et al., Characterization of Cu2ZnSnS4 thin film deposited by pulse laser deposition, 2017, pp. 1–6, vol. 40010.

[8] N.A. Bakr, S.A. Salman, S.A. Hameed, Deposition and characterization of Cu_2 $ZnSnS_4$ thin films for solar cell applications 13 (6) (2018) 3379–3388.

[9] Wei Wang, et al., Device characteristics of CZTSSe thin-film solar cells with 12.6% efficiency, Adv. Energy Mater. 4 (2014) 7.

[10] R. Hosseinpour, M. Izadifard, M.E. Ghazi, B. Bahramian, "Effect of annealing temperature on structural, optical, and electrical properties of sol–gel spin-coating-derived Cu_2ZnSnS_4 thin films, J. Electron. Mater. (2017).

[11] S.B. Patel, J.V. Gohel, Effect of type of solvent on the sol-gel spin coated CZTS thin films, Phys. Astron. Int. J. 1 (4) (2017) 1–5.

[12] J. Ge, et al., Improved performance of electroplated CZTS thin-film solar cells with bifacial configuration, ChemSusChem 9 (16) (2016) 2149–2158.

[13] A. Tang, Z. Li, F. Wang, M. Dou, Y. Pan, J. Guan, One step electrodeposition of Cu_2ZnSnS_4 thin films in a novel bath with sulfurization free annealing, Appl. Surf. Sci. 402 (Apr. 2017) 70–77.

[14] H. Yoo, J. Kim, Comparative study of Cu_2ZnSnS_4 film growth, Sol. Energy Mater. Sol. Cells 95 (1) (Jan. 2011) 239–244.

[15] A. Cazzaniga, et al., Ultra-thin Cu2ZnSnS4solar cell by pulsed laser deposition, Sol. Energy Mater. Sol. Cells 166 (March) (2017) 91–99.

[16] M. Beres, K.M. Yu, J. Syzdek, S.S. Mao, Stoichiometry control in Cu_2ZnSnS_4 thin films grown by pulsed laser deposition, Mater. Chem. Phys. 205 (2018) 90–96.

[17] Y. Shimamune, K. Jimbo, G. Nishida, M. Murayama, A. Takeuchi, H. Katagiri, Cu_2ZnSnS_4 formation by co-evaporation and subsequent annealing in S-flux using molecular beam epitaxy system, Thin Solid Films 638 (Sep. 2017) 312–317.

[18] Y. Zhao, D. Li, Z. Liu, Structural and elastic DFT study of four structures for Cu_2ZnSnS_4 under high pressure, J. Alloys Compd. 696 (2017) 86–95.

[19] L.A. Burton, Y. Kumagai, A. Walsh, F. Oba, DFT investigation into the underperformance of sulfide materials in photovoltaic applications, J. Mater. Chem. A 5 (19) (2017) 9132–9140.

[20] C. Li, Y. Li, B. Yao, G. Yang, Z. Ding, R. Deng, "Electronic and optical properties of kesterite Cu 2 ZnSnS 4 under in-plane biaxial strains : first-principles calculations, Phys. Lett. A 1 (2013) 1–5.

[21] F. Tran, P. Blaha, Accurate band gaps of semiconductors and insulators with a semilocal exchange-correlation potential, Phys. Rev. Lett. 102 (22) (2009) 5–8.

[22] Joachim Luitz, Peter Blaha, Karlheinz Schwarz, Georg K.H. Madsen, Dieter Kvasnicka, WIEN2k 1, 2017.

[23] F. Tran, P. Blaha, Accurate band gaps of semiconductors and insulators with a semilocal exchange-correlation potential, Phys. Rev. Lett. 102 (22) (2009) 5–8.

[24] J.P. Perdew, A. Ruzsinszky, J. Tao, V.N. Staroverov, G.E. Scuseria, G.I. Csonka, Prescription for the design and selection of density functional approximations: more constraint satisfaction with fewer fits, J. Chem. Phys. 123 (6) (2005).

[25] M. Mesbahi, M.L. Benkhedir, I.T. Conversion, A DFT STUDY of Quaternary Chalcogenide Semiconductors Cu2ZnSnS (Se)4 by Tran-Blaha Modified Becke-Johnson and Hubbard Potentials 79, 2017.

[26] E.R. Johnson, A.D. Becke, Communication: DFT treatment of strong correlation in 3d transition-metal diatomics, J. Chem. Phys. 146 (21) (2017).

[27] T.P. Sinha, et al., Optical and Electronic Structure Studies of Half Metallic in Sr_2 CoWO 6 Double Perovskite, 2017, pp. 2–5, vol. 140039.

[28] H. Khosravi, et al., DFT study of elastic, half-metallic and optical properties of Co_2 V(Al, Ge, Ga and Si) compounds 31 (2017).

[29] W. Zhang, J.R. Yin, X.Q. Tang, P. Zhang, Y.H. Ding, Density functional theory studies on the structural and physical properties of Cu-doped anatase TiO2(101) surface, Phys. E Low-dimens. Syst. Nanostruct. 85 (101) (2017) 259–263.

[30] L.C. Damonte, G.N. Darriba, M. Rentería, Structural and electronic properties of Al-doped ZnO semiconductor nanopowders: interplay between XRD and PALS experiments and first-principles/DFT modeling, J. Alloys Compd. 735 (2018) 2471–2478.

[31] F. Tran, J. Doumont, L. Kalantari, A.W. Huran, M.A.L. Marques, P. Blaha, Semilocal exchange-correlation potentials for solid-state calculations: current status and future directions, 2019, pp. 1–18.

[32] Y.F. Li, et al., Biaxial stress-dependent optical band gap, crystalline, and electronic structure in wurtzite ZnO: Experimental and ab initio study Biaxial stress-dependent optical band gap, crystalline, and electronic structure in wurtzite ZnO: experimental and ab *initio* study, J. Appl. Phys. 083516 (2008) (2013).

[33] G.K.H. Madsen, J. Carrete, M.J. Verstraete, BoltzTraP2, a Program for Interpolating Band Structures and Calculating Semi-classical Transport Coefficients, 2017.

[34] P. Bonazzi, L. Bindi, G.P. Bernardini, S. Menchetti, A model for the mechanism of incorporation of Cu, Fe and Zn in the stannite - Këesterite series, Cu2FeSnS4-Cu2ZnSnS4, Can. Mineral. 41 (3) (2003) 639–647.

[35] S.R. Hall, J.T. Szymanski, J.M. Stewart, Kesterite, $Cu_2(Zn,Fe)SnS_4$ and Stannite $Cu_2(Fe,Zn)SnS_4$, structurally similar but distinct minerals, Can. Mineral. 16 (2) (1978) 131–137 [Online]. Available, http://canmin.geoscienceworld.org/cgi/content/abstract/16/2/131.

[36] A. Ghosh, R. Thangavel, Experimental and theoretical study of structural and optical properties of Cu_2ZnSnS_4 nanocrystals for solar photovoltaic applications, Energy Environ. Focus 3 (2) (2014) 157–161.

[37] M. Wei, Q. Du, D. Wang, W. Liu, G. Jiang, C. Zhu, Synthesis of spindle-like kesterite Cu_2ZnSnS_4 nanoparticles using thiourea as sulfur source, Mater. Lett. 79 (2012) 177–179.

[38] F.D. Murnaghan, Te compressibility of media under extreme pressures, Proc. Nat. Acad. Sci. U.S.A. 30 (1944) 244–247.

[39] G.L. Agawane, S.W. Shin, S.A. Vanalakar, A.V. Moholkar, J.H. Kim, Next generation promising $Cu_2(ZnxFe1-x)SnS_4$ photovoltaic absorber material prepared by pulsed laser deposition technique, Mater. Lett. 137 (December) (2014) 147–149.

[40] H. Katagiri, N. Sasaguchi, S. Hando, S. Hoshino, J. Ohashi, T. Yokota, Preparation and evaluation of Cu_2ZnSnS_4 thin films by sulfurization of E-B evaporated precursors, Sol. Energy Mater. Sol. Cells 49 (1–4) (1997) 407–414.

[41] J.P. Leitão, et al., Photoluminescence and electrical study of fluctuating potentials in Cu_2ZnSnS_4-based thin films, Phys. Rev. B - Condens. Matter Mater. Phys. 84 (2) (2011) 1–8.

[42] Y.B.K. Kumar, V.S. Raja, Investigations on the growth of Cu_2ZnSnS_4 thin films for solar cell absorber layer, Surface. Interfac. 9 (2017) 233–237.

[43] S.A. Khalate, R.S. Kate, R.J. Deokate, Chemical spray Pyrolyzed Kesterite Cu_2ZnSnS_4 (CZTS) Thin Films, 2018, p. 80009.

[44] J. Robin, Influence de la pression sur quelques propriétés des semiconducteurs, J. Phys. le Radium 21 (2) (1960) 130–140.

[45] H.Y. Fan, M.L. Shepherd, W. et Spitzer, Photoconductivity Conference, New York, 1956.

[46] M. Boujnah, M. Boumdyan, S. Naji, A. Benyoussef, A. El Kenz, M. Loulidi, High efficiency of transmittance and electrical conductivity of v doped ZnO used in solar cells applications, J. Alloys Compd. 671 (2016) 560–565.